Interpreting Frame Transformations in AC Systems as Diagonalization of Harmonic Transfer Functions

Yitong Li *Student Member, IEEE*, Yunjie Gu *Member, IEEE*, Timothy C. Green *Fellow, IEEE*

***Abstract*—Analysis of ac electrical systems can be performed via frame transformations in the time-domain or via harmonic transfer functions (HTFs) in the frequency-domain. The two approaches each have unique advantages but are hard to reconcile because the coupling effect in the frequency-domain leads to infinite dimensional HTF matrices that need to be truncated. This paper explores the relation between the two representations and shows that applying a frame transformation on the input-output signals creates a direct equivalence to a similarity transformation to the HTF matrix of the system. Under certain conditions, such similarity transformations have a diagonalizing effect which, essentially, reduces the HTF matrix order from infinity to two or one, making the matrix tractable mathematically without truncation or approximation. This theory is applied to a droop-controlled voltage source inverter as an illustrative example. A stability criterion is derived in the frequency-domain which agrees with the conventional state-space model but offers greater insights into the mechanism of instability in terms of the negative damping (non-passivity) under droop control. Therefore, the paper not only establishes a unified view in theory but also offers an effective practical tool for stability assessment.**

***Index Terms*—Harmonic State Space, Harmonic Transfer Function, Frame Transformation, Matrix Diagonalization, Droop Control**

I. Introduction

Frame transformations play a central role in modeling and analysis of three-phase ac electrical systems. There are three types of basic transformations: Clarke transformation [1], complex transformation [2]–[4], and rotation transformation [5]. Other transformations (Ku transformation, symmetric component transformation, and forward-backward transformation) prove to be combinations of the basic ones [6]. The three basic transformations each play an important yet different role in simplifying the model of ac electrical systems. The Clarke transformation separates the common-mode components which does not affect power transmission; the complex transformation reduces a vector model to a scalar model (but only for symmetric systems); the rotation transformation transforms an ac sinusoidal system to a dc equivalent one. Due to these benefits, frame transformations have been successfully used in power engineering for more than a century.

On the other hand, the practical benefits of such transformations is limited to three-phase balanced sinusoidal systems, since unbalanced and non-sinusoidal systems induce time-varying operating points in the rotating frame, which implies time-varying state equations after linearization. Unbalanced and non-sinusoidal systems are becoming increasingly widespread in power systems because of the emergence of distributed generation interfaced by power electronic converters, which is often single-phase and inevitably creates harmonic distortions [7]–[10].

To solve this problem, an alternative approach based on harmonic state space (HSS) theory has gained attention. This theory was first proposed in the 1990s [11]–[13] and introduced into the power engineering community in the 2000s [7], [14], [15]. The HSS method models an ac system directly in the stationary frame and represents the ac dynamics by the frequency coupling in the corresponding harmonic transfer function (HTF). It provides a general framework to address unbalanced and non-sinusoidal ac systems since an HTF can include higher-order harmonic extension beyond fundamental positive-sequence operating points. However, it is difficult to use HSS models to analysis a composite system with interaction between multiple sub-systems, as this relates to algebraic operations (summation, multiplication, and inversion) on HTF matrices which is infinite-order and intractable mathematically. Approximations have to be made to render it tractable, which are often based on heuristics with no theoretic guarantee [16], [17].

It is clear that the frame transformation method and the HSS method each have their own advantages and disadvantages. A unified view of the two could help circumvent the difficulties of each on its own, and this is the intended the contribution of this paper. In particular, we point out that frame transformations in the time-domain are equivalent to similarity transformations on an HTF matrix in the frequency-domain. Under certain conditions, such similarity transformations have a diagonalizing effect on an HTF matrix, which takes place in two steps: i) block diagonalization (via rotation transformation) to eliminate the frequency coupling effect; and ii) entry diagonalization (via complex transformation) to reduce an HTF matrix to a scalar. These matrix diagonalization essentially reduce the order of an HTF matrix from infinity to two and then one, making the transfer function tractable mathematically. The reduced HTF matrix is shown to be exactly equivalent to conventional transfer functions derived directly in the rotating and complex frames.

Following the theoretic discussion, a case study is presented on a droop-controlled voltage source inverter (VSI). The HTF model of the VSI is obtained in the stationary frame, and then transformed to the synchronous frame according to the proposed diagonalization law. It is discovered that the HTF of the droop-controlled VSI contain two parts. The first part rep-

Yitong Li, Yunjie Gu and Timothy C. Green are with the Department of Electrical and Electronic Engineering, Imperial College London. E-mail: yitong.li15@imperial.ac.uk; yunjie.gu@imperial.ac.uk; t.green@imperial.ac.uk.

This work was supported by the Engineering and Physical Sciences Research Council of UK (EPSRC) under award EP/S000909/1.

resents the current dynamics in a simple inductance-resistance format and can be entry-diagonalized. The second part represents the droop dynamics and is only block-diagonalizable, but the interaction between the diagonal and off-diagonal entries is very weak and proves to be negligible. These results yield a frequency-domain stability criterion which agrees with the results in [18], [19], but provides more insights into the mechanism of instability in terms of the negative damping (non-passivity) in droop control. All major conclusions of the paper are verified by experiments.

The paper is organized as follows. The principle of HSS and HTF in introduced briefly in Section II. The relationship between frame transformation and the diagonalization of an HTF matrix (and order-reduction achieved) is presented in Section III. The case study on a droop-controlled VSI is given in Section IV. The last section concludes the paper.

II. Harmonic State Space and Harmonic Transfer Function

Consider a general non-linear dynamic system with state x, input u and output y (x, u, and y are all column vectors)

$$\begin{aligned} \dot{x} &= f(x,u) \\ y &= g(x,u). \end{aligned} \tag{1}$$

In small-signal analysis, we linearize this system by taking the partial derivative of f and g around the equilibrium operating point $x_e(t)$ and $u_e(t)$. That is,

$$\begin{aligned} \dot{\hat{x}} &= A(t)\hat{x} + B(t)\hat{u} \\ \hat{y} &= C(t)\hat{x} + D(t)\hat{u} \end{aligned} \tag{2}$$

where

$$\begin{pmatrix} A(t) & B(t) \\ C(t) & D(t) \end{pmatrix} = \left.\frac{\partial(f,g)}{\partial(x,u)}\right|_{x_e(t),u_e(t)} \tag{3}$$

is the Jacobian matrix and $\hat{}$ denotes the small-signal variation. For a dc system, the operating point is defined by constant values of $x_e(t)$ and $u_e(t)$ and so $A(t)$, $B(t)$, $C(t)$ and $D(t)$ are also constant and the system defined in (2) is linear time invariant (LTI). For an ac system, on the other hand, $x_e(t)$ and $u_e(t)$ are periodically time-varying and so are $A(t)$, $B(t)$, $C(t)$ and $D(t)$, which gives rise to a linear time periodic (LTP) system [11], [12], [20], [21]. One important difference between LTI and LTP is that a LTP system has a frequency-coupling feature in which multiple terms of related frequencies can be generated in the output y even when the input u is a single-frequency signal. This effect can be represented mathematically through an HSS and HTF model [11], [12].

Expanding $A(t)$, $B(t)$, $C(t)$, and $D(t)$ into Fourier series, we can re-write (2) as

$$\begin{aligned} \dot{\hat{x}} &= \sum A_n e^{jn\omega_p t}\hat{x} + \sum B_n e^{jn\omega_p t}\hat{u} \\ \hat{y} &= \sum C_n e^{jn\omega_p t}\hat{x} + \sum D_n e^{jn\omega_p t}\hat{u} \end{aligned} \tag{4}$$

in which A_n, B_n, C_n and D_n are the Fourier coefficients of $A(t)$, $B(t)$, $C(t)$ and $D(t)$ respectively, ω_p is the fundamental frequency, and the summation, $\sum$, sums from $n=-\infty$ to $+\infty$. Taking a Laplace transform of (4), we have

$$\begin{aligned} s\hat{x}(s) &= \sum A_n \hat{x}(s-jn\omega_p) + \sum B_n \hat{u}(s-jn\omega_p) \\ \hat{y}(s) &= \sum C_n \hat{x}(s-jn\omega_p) + \sum D_n \hat{u}(s-jn\omega_p) \end{aligned} \tag{5}$$

Replacing s by $s+jk\omega_p$ with an arbitrary integer k, we can get

$$\begin{aligned} s_k\hat{x}(s_k) &= \sum_n A_{n+k}\hat{x}(s_{-n}) + \sum_n B_{n+k}\hat{u}(s_{-n}) \\ \hat{y}(s_k) &= \sum_n C_{n+k}\hat{x}(s_{-n}) + \sum_n D_{n+k}\hat{u}(s_{-n}) \end{aligned} \tag{6}$$

Here we make use of the notation $s_n = s + jn\omega_p$ for brevity. Let the integer k traverse from $-\infty$ to $+\infty$ and the resulted equations can be written in the form of infinite matrices:

$$\begin{aligned} s\mathcal{X} &= (\mathcal{A}-\mathcal{N})\mathcal{X} + \mathcal{B}\mathcal{U} \\ \mathcal{Y} &= \mathcal{C}\mathcal{X} + \mathcal{D}\mathcal{U} \end{aligned} \tag{7}$$

where

$$\mathcal{X} = \begin{pmatrix} \vdots \\ \hat{x}(s_1) \\ \hat{x}(s) \\ \hat{x}(s_{-1}) \\ \vdots \end{pmatrix},\ \mathcal{A} = \begin{pmatrix} \ddots & & & & \iddots \\ & A_0 & A_1 & A_2 & \\ & A_{-1} & A_0 & A_1 & \\ & A_{-2} & A_{-1} & A_0 & \\ \iddots & & & & \ddots \end{pmatrix}. \tag{8}$$

$\mathcal{X}$ is the harmonic extension of $\hat{x}(s)$, and $\mathcal{A}$ in such a form is called an infinite Toeplitz matrix [11], [12]. $\mathcal{U}$ and $\mathcal{Y}$ are defined in a similar way to $\mathcal{X}$, and $\mathcal{B}$, $\mathcal{C}$ and $\mathcal{D}$ are defined in a similar way to $\mathcal{A}$. $\mathcal{N} = \text{blkdiag}(jn\omega_p I)$ is a block-diagonal matrix with I being an identity matrix of the same dimension an A. Equation (7) is called a harmonic state space (HSS) model, from which follows the harmonic transfer function (HTF)

$$\mathcal{Y} = \mathcal{G}\mathcal{U} \tag{9}$$

in which

$$\mathcal{G} = \mathcal{C}(s\mathcal{I} + \mathcal{N} - \mathcal{A})^{-1}\mathcal{B} + \mathcal{D}. \tag{10}$$

Equation (9) can also be written in an expanded form as

$$\begin{pmatrix} \vdots \\ \hat{y}(s_1) \\ \hat{y}(s) \\ \hat{y}(s_{-1}) \\ \vdots \end{pmatrix} = \begin{pmatrix} \ddots & & & & \iddots \\ & G_0(s_1) & G_1(s_1) & G_2(s_1) & \\ & G_{-1}(s) & G_0(s) & G_1(s) & \\ & G_{-2}(s_{-1}) & G_{-1}(s_{-1}) & G_0(s_{-1}) & \\ \iddots & & & & \ddots \end{pmatrix} \begin{pmatrix} \vdots \\ \hat{u}(s_1) \\ \hat{u}(s) \\ \hat{u}(s_{-1}) \\ \vdots \end{pmatrix}. \tag{11}$$

To reveal the frequency-coupling effect represented by the HTF matrix, we find $\hat{y}(s)$ from (11)

$$\hat{y}(s) = \sum G_n(s)\hat{u}(s_{-n}). \tag{12}$$

Letting $s = j\omega$, we get the frequency spectrum of $\hat{y}$

$$\hat{y}(j\omega) = \sum G_n(j\omega)\hat{u}(j\omega_{-n}) \tag{13}$$

where $\omega_n = \omega + n\omega_p$. Suppose the input $\hat{u}$ has a single frequency ω_u, that is, $\hat{u} = Ue^{j\omega_u t}$ where U is the amplitude

vector. The corresponding spectrum is $\hat{u}(j\omega) = U\delta(\omega - \omega_u)$ and

$$\begin{aligned}\hat{y}(j\omega) &= \sum G_n(j\omega)U\delta(\omega_{-n} - \omega_u) \\ &= \sum G_n(j\omega)U\delta(\omega - \omega_u - n\omega_p)\end{aligned} \tag{14}$$

where $\delta(\omega)$ is the Dirac function. It is clear from (14) that multiple frequencies $\omega_u + n\omega_p$ appear in the output spectrum under single-frequency input, as illustrated in Fig. 1. This frequency-coupling effect causes a fundamental difficulty. As illustrated in Fig. 2, when two or more sub-systems are connected in a closed loop (e.g. a voltage source converter connected to a synchronous generator), the back-and-forth interaction between them generates infinitely many harmonic terms. Their interaction has to be analysed using the algebra of infinite-order HTF matrices and this is intractable.

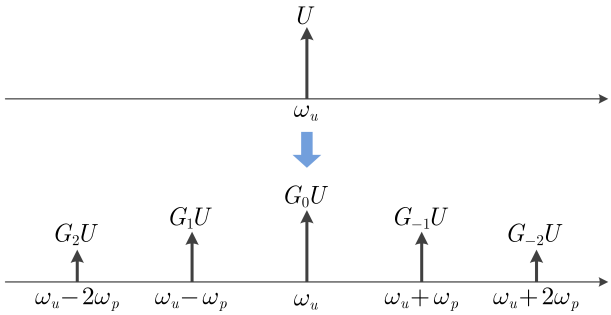

Fig. 1. The frequency coupling effect in a LTP system: a single-frequency input generates multiple frequencies in the output through the multiple entries in $\mathcal{G}$.

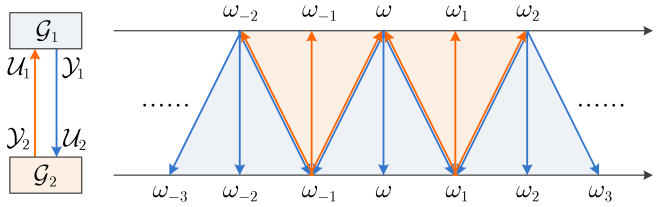

Fig. 2. Illustration of infinite harmonic reflection in an interconnected LTP system. $\mathcal{G}_1$ and $\mathcal{G}_2$ are interconnected such that the output of one is applied as the input of the other and *vice versa*. Such an interconnection is common in power system analysis: $\mathcal{G}_1$ could be a voltage source such that it outputs a voltage and has current as an input (Thevenin format using an impedance model) whereas $\mathcal{G}_2$ is a current sink such that it outputs a current and has voltage as an input (Norton format using an admittance model). Their harmonic interaction determines the small-signal stability of the interconnected system.

Further consideration reveals that the frequency coupling is caused by only the non-diagonal elements of the HTF. In the light of this observation, the frequency-coupling effect could be eliminated if the HTF matrix could be diagonalized and the overall solution would be tractable. This diagonalization can be realized by frame transformations in the time-domain, as will be explained in the following sections.

III. Frame Transformation and Matrix Diagonalization

Before describing the diagonalization in detail, we first define two types of diagonal HTF matrix, as shown in Fig. 3. The first type is *block diagonal*, for which the matrix is made up of a diagonal series of $\dim(u) \times \dim(y)$ blocks. In this form, there is no frequency coupling present but the various elements of u and y are coupled representing a multi-input-multi-output (MIMO) system. The second form, *entry diagonal*, is completely diagonalized entry-wise and represents a series of decoupled single-input-single-output (SISO) scalar systems. The input u and output y are assumed to have the same dimension here as is the case for most electrical circuits.

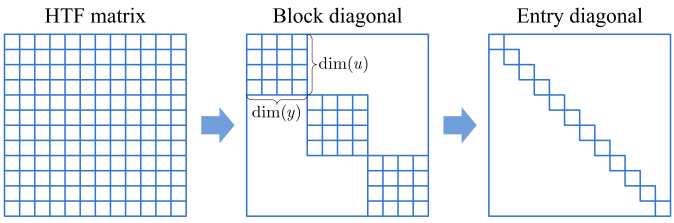

Fig. 3. Definition of two forms of diagonal HTF matrix: block diagonal and entry diagonal.

We now demonstrate the relationship between a frame transformation and HTF matrix diagonalization. Consider a general frame transformation $T(t)$ in the time-domain on u and y. The vectors in the new frame are

$$u'(t) = T(t)u(t),\ y'(t) = T(t)y(t) \tag{15}$$

where $T(t)$ is a periodical transformation function. Representing $T(t)$ as a Toeplitz matrix as in (8), we get

$$\mathcal{U}' = \mathcal{T}\mathcal{U},\ \mathcal{Y}' = \mathcal{T}\mathcal{Y} \tag{16}$$

where

$$\mathcal{T} = \begin{pmatrix} \ddots & & & & \iddots \\ & T_0 & T_1 & T_2 & \\ & T_{-1} & T_0 & T_1 & \\ & T_{-2} & T_{-1} & T_0 & \\ \iddots & & & & \ddots \end{pmatrix} \tag{17}$$

and T_n is $T(t)$'s Fourier coefficient. Combining (16) and (9), we get the HTF $\mathcal{G}'$ in the new frame

$$\mathcal{G}' = \mathcal{T}\mathcal{G}\mathcal{T}^{-1}. \tag{18}$$

It is clear that (18) defines a similarity transformation between $\mathcal{G}'$ and $\mathcal{G}$ via $\mathcal{T}$. That is, a frame transformation in the time-domain is equivalent to a similarity transformation in an HTF. If $T(t)$ is properly selected, an HTF matrix may be diagonalized with such a transformation.

A general scheme for finding a diagonalizing transformation is given by the Floquet's theorem [11]. In this paper, we focus on two particular transformations widely used in three-phase ac power system analysis: the rotation and complex transformations, which are summarized in Fig. 4 and in which $\alpha\beta$ and dq refer to the stationary and rotating frames respectively, and $\alpha\beta\pm$ and $dq\pm$ are the corresponding complex frames.

The rotation transformation T_r and complex transformation T_j builds the relationships between these frames:

$$\begin{pmatrix} u_{\alpha\beta+} \\ u_{\alpha\beta-} \end{pmatrix} = T_j \begin{pmatrix} u_\alpha \\ u_\beta \end{pmatrix}, \quad \begin{pmatrix} u_d \\ u_q \end{pmatrix} = T_j^{-1} \begin{pmatrix} u_{dq+} \\ u_{dq-} \end{pmatrix}, \quad \begin{pmatrix} u_{dq+} \\ u_{dq-} \end{pmatrix} = T_r \begin{pmatrix} u_{\alpha\beta+} \\ u_{\alpha\beta-} \end{pmatrix} \tag{19}$$

in which

$$T_j = \begin{pmatrix} 1 & j \\ 1 & -j \end{pmatrix}, \; T_r = \begin{pmatrix} e^{-j\omega_p t} & 0 \\ 0 & e^{j\omega_p t} \end{pmatrix}. \tag{20}$$

Combining T_r and T_j gives the real-signal rotation transformation T_p which is commonly known as the Park transformation

$$T_p = T_j^{-1} T_r T_j = \begin{pmatrix} \cos\omega_p t & \sin\omega_p t \\ -\sin\omega_p t & \cos\omega_p t \end{pmatrix}. \tag{21}$$

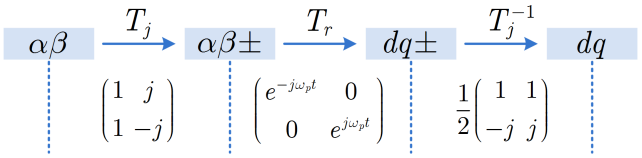

Fig. 4. Summary of reference frames and transformations in between used in three-phase ac power systems.

We further show that T_r has a block-diagonalizing effect on HTF matrices. The Fourier series expansion of T_r is

$$T_r = \begin{pmatrix} e^{-j\omega_p t} & 0 \\ 0 & e^{j\omega_p t} \end{pmatrix} = \underbrace{\begin{pmatrix} 0 & 0 \\ 0 & 1 \end{pmatrix}}_{T_{r1}} e^{j\omega_p t} + \underbrace{\begin{pmatrix} 1 & 0 \\ 0 & 0 \end{pmatrix}}_{T_{r-1}} e^{-j\omega_p t}. \tag{22}$$

In other words,

$$T_{r1} = \begin{pmatrix} 0 & 0 \\ 0 & 1 \end{pmatrix}, \; T_{r-1} = \begin{pmatrix} 1 & 0 \\ 0 & 0 \end{pmatrix}, \text{ and } \; T_{rn} = \begin{pmatrix} 0 & 0 \\ 0 & 0 \end{pmatrix} \text{ for } n \neq \pm 1 \tag{23}$$

from which follows the Toeplitz matrix $\mathcal{T}_r$ according to (17)

$$\mathcal{T}_r = \begin{pmatrix} \ddots & & & & & \\ & 0 & 0 & & & \\ & 0 & 1 & & & \\ & 1 & 0 & & 0 & 0 \\ & 0 & 0 & & 0 & 1 \\ & & & 1 & 0 & \\ & & & 0 & 0 & \\ & & & & & \ddots \end{pmatrix} \tag{24}$$

where blanks indicate zeros. This matrix links the HTF in the $\alpha\beta\pm$ and $dq\pm$ frame by

$$\mathcal{G}_{dq\pm} = \mathcal{T}_r \mathcal{G}_{\alpha\beta\pm} \mathcal{T}_r^{-1}, \; \mathcal{G}_{\alpha\beta\pm} = \mathcal{T}_r^{-1} \mathcal{G}_{dq\pm} \mathcal{T}_r. \tag{25}$$

Notably, $\mathcal{T}_r$ is a permutation matrix, so the transformations in (25) rearrange the positions of the HTF entries without changing their values. Applying (25) to a three-phase balanced ac system, we get the relationship in Fig. 5. It is clear that the entries of $\mathcal{G}_{dq\pm}$ are the same as those of $\mathcal{G}_{\alpha\beta\pm}$, but are rearranged into a block-diagonal form. This means that the rotation transformation has a block-diagonalizing effect on the HTF matrix provided that the system is three-phase balanced. The zero-axis signal can be readily included into the diagonlization process as it is independent of both dq and $\alpha\beta$. The corresponding transformation is similar to Fig. 5 but not as concise, and is therefore not shown here for the sake of brevity.

From $\mathcal{G}_{\alpha\beta\pm}$ in Fig. 5, we can readily obtain the entry-wise expression

$$\begin{aligned} y_{\alpha\beta+}(s_1) &= G_{11}(s) u_{\alpha\beta+}(s_1) + G_{12}(s) u_{\alpha\beta-}(s_{-1}) \\ y_{\alpha\beta-}(s_{-1}) &= G_{21}(s) u_{\alpha\beta+}(s_1) + G_{22}(s) u_{\alpha\beta-}(s_{-1}) \end{aligned} \tag{26}$$

which can be written as a 2×2 matrix

$$\begin{pmatrix} y_{\alpha\beta+}(s_1) \\ y_{\alpha\beta-}(s_{-1}) \end{pmatrix} = \begin{pmatrix} G_{11}(s) & G_{12}(s) \\ G_{21}(s) & G_{22}(s) \end{pmatrix} \begin{pmatrix} u_{\alpha\beta+}(s_1) \\ u_{\alpha\beta-}(s_{-1}) \end{pmatrix}. \tag{27}$$

Equation (27) contains all essential information of $\mathcal{G}_{\alpha\beta\pm}$ since the other entries can be obtained by shifting s to s_n ($n = 1, -1, 2, -2, \cdots$). In particular, if we shift from s to s_{-1}, we get the same model as the one proposed in [10] which has been recognized as a unified model in the stationary frame:

$$\begin{pmatrix} y_{\alpha\beta+}(s) \\ y_{\alpha\beta-}(s_{-2}) \end{pmatrix} = \begin{pmatrix} G_{11}(s_{-1}) & G_{12}(s_{-1}) \\ G_{21}(s_{-1}) & G_{22}(s_{-1}) \end{pmatrix} \begin{pmatrix} u_{\alpha\beta+}(s) \\ u_{\alpha\beta-}(s_{-2}) \end{pmatrix}. \tag{28}$$

The shifted s in (27) and (28) also clearly show the frequency coupling effect, which implies the LTP nature of the system in the stationary reference frame.

Further to the rotation transformation T_r, the complex transformation T_j (and its Toeplitz form $\mathcal{T}_j$) define the linkage between the real ($\alpha\beta$, dq) and complex ($\alpha\beta\pm$, $dq\pm$) frames

$$\begin{aligned} \mathcal{G}_{dq\pm} &= \mathcal{T}_j \mathcal{G}_{dq} \mathcal{T}_j^{-1}, \quad \mathcal{G}_{dq} = \mathcal{T}_j^{-1} \mathcal{G}_{dq\pm} \mathcal{T}_j \\ \mathcal{G}_{\alpha\beta\pm} &= \mathcal{T}_j \mathcal{G}_{\alpha\beta} \mathcal{T}_j^{-1}, \quad \mathcal{G}_{\alpha\beta} = \mathcal{T}_j^{-1} \mathcal{G}_{\alpha\beta\pm} \mathcal{T}_j \end{aligned}. \tag{29}$$

Since T_j is constant, its Fourier series only contains 0^{th} harmonics. According to (17), the corresponding Toeplitz matrix is

$$\mathcal{T}_j = \begin{pmatrix} \ddots & & & \\ & T_j & & \\ & & T_j & \\ & & & \ddots \end{pmatrix} \tag{30}$$

This indicates that $\mathcal{T}_j$ is block-diagonal itself and does not change the block arrangement of an HTF matrix, that is, an HTF matrix is block-diagonal in a real frame if and only if its complex-frame counterpart is block-diagonal as well. Nonetheless, T_j has entry-diagonalizing effect on a block-diagonal HTF matrix, as shown below. As $\mathcal{G}_{dq}$, $\mathcal{G}_{dq\pm}$ and $\mathcal{T}_j$

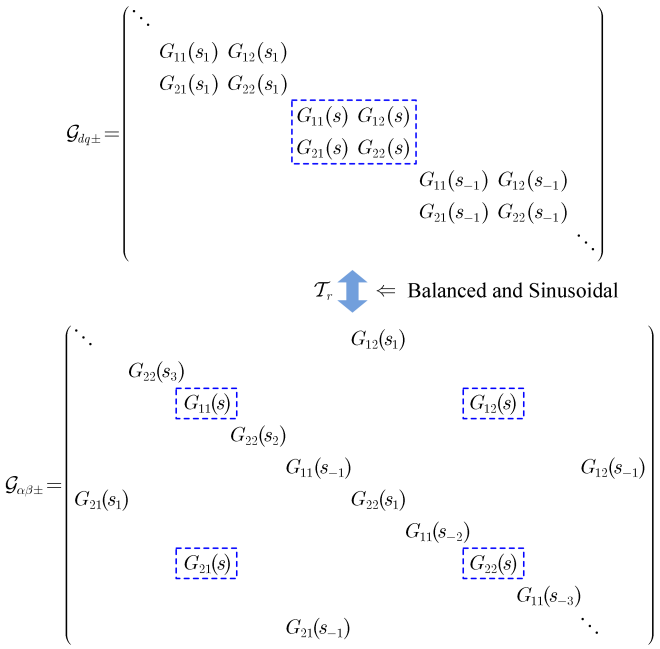

Fig. 5. Block-diagonalization of HTF matrix through rotation transformation.

are all block-diagonal, we can evaluate their relationships just using an arbitrary block

$$\underbrace{\begin{pmatrix} G_{11} & G_{12} \\ G_{21} & G_{22} \end{pmatrix}}_{\mathcal{G}_{dq\pm}\text{ block}} = \underbrace{\begin{pmatrix} 1 & j \\ 1 & -j \end{pmatrix}}_{\mathcal{T}_j\text{ block}} \cdot \underbrace{\begin{pmatrix} G_{dd} & G_{dq} \\ G_{qd} & G_{qq} \end{pmatrix}}_{\mathcal{G}_{dq}\text{ block}} \cdot \underbrace{\frac{1}{2}\begin{pmatrix} 1 & 1 \\ -j & j \end{pmatrix}}_{\mathcal{T}_j^{-1}\text{ block}} . \tag{31}$$

If $\mathcal{G}_{dq}$ meets the following condition

$$G_{dd} = +G_{qq},\ G_{dq} = -G_{qd} \tag{32}$$

then (31) can be simplified as

$$G_{11} = G_{dd} - jG_{dq},\ G_{11} = G_{dd} + jG_{dq},\ G_{12} = G_{21} = 0 \tag{33}$$

so $\mathcal{G}_{dq\pm}$ turns out to be entry-diagonal. This relationship is illustrated in Fig. 6 and the condition in (32) is called the symmetric condition, since it implies that the d and q axis are exchangeable. In real systems, asymmetry is often induced by the saliency of generators and the asymmetric outer control loops (e.g. phase-locked loop, droop control loop, and dc-link control loop) of power electronic converters [22], [23]. For such asymmetric systems, the symmetric condition is not satisfied which hampers entry-diagonalization, but we shall show later that quasi-symmetric can be defined where the asymmetry does not effect stability and is therefore negligible.

After the HTF matrix is diagonalized, algebraic operation (summation, multiplication, inversion) can be performed block-wise or entry-wise and through this computation is greatly simplified. Moreover, each of the diagonal blocks or entries contains the full information of the HTF matrix since other blocks or entries are replications with a frequency shift (Fig. 5) or complex conjugates (Fig. 6), which means that a single block or entry can be used as a reduced-order but full-information representation for the whole HTF matrix. In such a

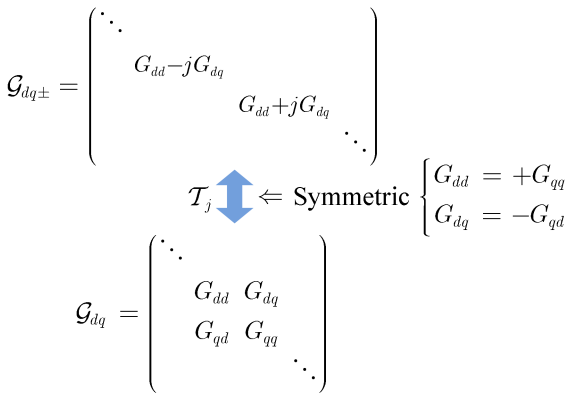

Fig. 6. Entry-diagonalization of HTF matrix through complex transformation.

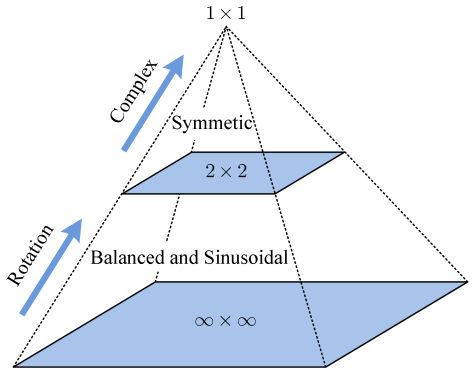

Fig. 7. Rotation and complex frame transformations form a pyramid of diagonalization and order reduction on HTF matrix.

way, we give a frequency-domain interpretation of how frame transformation helps to simplify the representation of an ac system in the sense of HTF matrix diagonalization and order-reduction. This is summarize as a pyramid diagram in Fig. 7.

It needs to be pointed out that there are strict conditions for a system to be diagonalizable using basic transformations. The block-diagonalization via rotation transformation is only feasible for three-phase balanced sinusoidal systems, and not feasible for unbalanced (e.g. single-phase) or non-sinusoidal (e.g. diode rectifier) systems. The entry-diagonalization via complex transformation is only feasible for symmetric systems, meaning the d and q (or α and β) axis have reciprocal dynamics. However, it might be possible to find new transformations for the diagonalization of asymmetric, unbalanced, or non-sinusoidal systems, which opens up a new direction of future works.

IV. Stability Relationship

As explained in the preceding section, the rotation and complex transformations lead to the diagonalization and therefore order-reduction of the HTF matrix. This section explores the stability relationships between the original and the diagonalized reduced-order system.

We first investigate block-diagonalization. It is clear from Fig. 5 that all dynamics of the system are captured by the central block of $\mathcal{G}_{dq\pm}$ (marked in the dashed box in Fig. 5), and

other elements in the HTF matrix are derived via frequency shifting on the central elements (that is, replacing s by $s_n = s + jn\omega_p$). Since the poles and zeros replicate with an offset of s, we get the pole/zero relationship in Fig. 8 [11], [12], [20], [21]. The poles/zeros in the fundamental strip of the s-plane are associated with the reduced-order system, and the ones in the complementary strips are associated with the original system. The poles/zeros in the fundamental strip and the ones in the complementary strips have the same real part, and therefore carry the same information concerning stability.

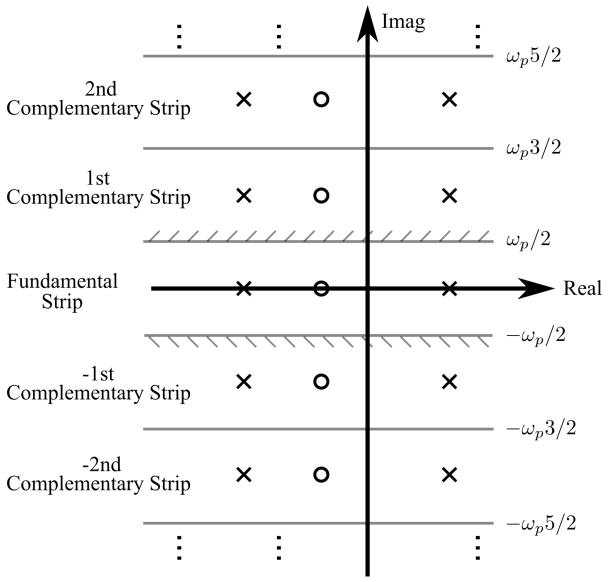

Fig. 8. Pole/zero relationship of the original HTF matrix and the reduced-order central block [12].

Now we look into entry-diagonalization. Equations (31) (33) and Fig. 6 show that the diagonal entries of $\mathcal{G}_{dq\pm}$ are the linear combination of the original entries of $\mathcal{G}_{dq}$, so the poles are unchanged in the transformation, but the zeros may not be. Zeros do not affect open-loop stability directly but may affect the stability in a closed-loop system since feedback interaction may reflect zeros into poles. Therefore, we need to evaluate the impact of entry-diagonalization in the stability a closed-loop system. We assume two sub-systems $\mathcal{G}$ and $\mathcal{H}$ connected via negative feedback, as illustrated in Fig. 9(a). This is a two-input-two-output (TITO) system but can be reduced to two single-input-single-output (SISO) systems if both $\mathcal{G}$ and $\mathcal{H}$ meet the symmetric condition (entry-diagonalizable), as shown in Fig. 9(b). The two SISO systems are in conjugation so their poles have opposite imaginary parts and an identical real part, indicating that either of them can be used to evaluate the stability of the whole system. If $\mathcal{G}$ or $\mathcal{H}$ is not symmetric, this order-reduction no longer holds and matrix determinant or eigenvalues needs to be used to evaluate stability [22]–[24]. Such methods use brute-force calculation and lose the connection to the loop-structure of the system. To overcome this problem, a different approach is proposed here which decomposes the determinant of a TITO system into symmetric and asymmetric loops.

The TITO feedback system in Fig. 9(a) can be equivalently

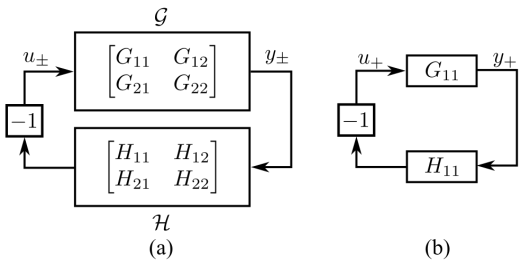

Fig. 9. Two systems interconnected via negative feedback. (a) Block-diagnolization case, i.e., TITO system. (b) Entry-diagnolization case, i.e., SISO system (only the $+$ loop is shown because the $+$ and $-$ loops are complex conjugate and hold the same information on stability).

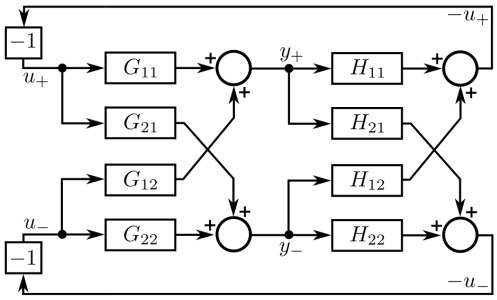

Fig. 10. Scalar block diagram for the closed-loop system.

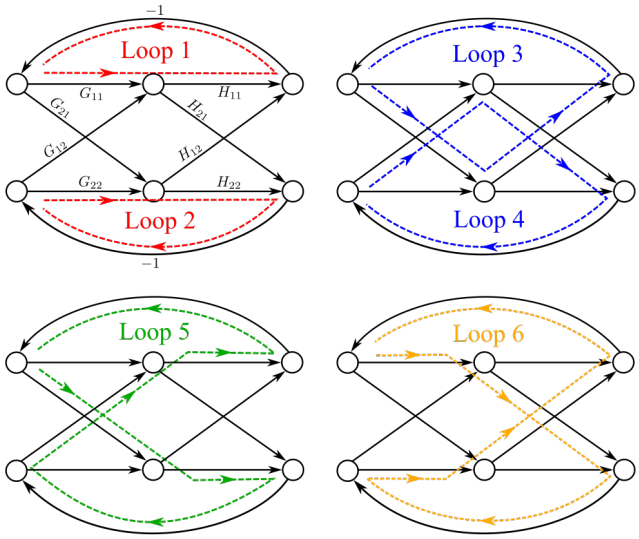

Fig. 11. Signal flow diagram of the closed-loop system.

converted to the scalar block diagram in Fig. 10, and further to the signal flow diagram in Fig. 11. From the signal flow diagram, we identify six independent loops whose loop gains are

$$\begin{aligned} l_1 &= -G_{11}H_{11},\ l_2 = -G_{22}H_{22} \\ l_3 &= -G_{21}H_{12},\ l_4 = -G_{12}H_{21} \\ l_5 &= G_{21}H_{22}G_{12}H_{11} \\ l_6 &= G_{11}H_{21}G_{22}H_{12} \end{aligned} \tag{34}$$

According to the Mason's gain formula [25], [26], the deter-

minant (i.e., the characteristic equation) of the system equals

$$\Delta = 1 - (l_1 + l_2 + l_3 + l_4 + l_5 + l_6) + (l_1 l_2 + l_3 l_4) \quad (35)$$

which can be rearranged as

$$\Delta = \underbrace{(1-l_1)(1-l_2)}_{\text{symmetric loop}} \underbrace{\left[1 + \frac{(1-l_3)(1-l_4) - (1+l_5+1_6)}{(1-l_1)(1-l_2)}\right]}_{\text{asymmetric loop}} \quad (36)$$

Hence, we decompose the determinant into three loops, whose loop gains equal $-l_1$, $-l_2$, and $\frac{(1-l_3)(1-l_4)-(1+l_5+l_6)}{(1-l_1)(1-l_2)}$ respectively. The first two loops exactly coincides with the loops of a symmetric system and are therefore called symmetric loops, whereas the third loop appears only in asymmetric systems and is called the asymmetric loop. If the asymmetric loop itself is stable, the stability of the system is only determined by its symmetric loops, and we call such a system *quasi-symmetric*.

In many practical cases, $\mathcal{G}$ is asymmetric but $\mathcal{H}$ is symmetric (e.g., the case study given in next section), or vise versa. When $\mathcal{H}$ is symmetric, $H_{12} = H_{21} = 0$ and loop gains $l_3 = l_4 = l_6 = 0$. Then (36) can be simplified as

$$\Delta = \underbrace{(1-l_1)(1-l_2)}_{\text{symmetric loop}} \underbrace{\left[1 + \frac{-l_5}{(1-l_1)(1-l_2)}\right]}_{\text{asymmetric loop}} \quad (37)$$

It is clear that the asymmetric loop is simplified compared to (36) and hence the quasi-symmetric condition is also simplified. To give the reader a more intuitive illustration, (37) is visualized via block transformation in Fig. 12.

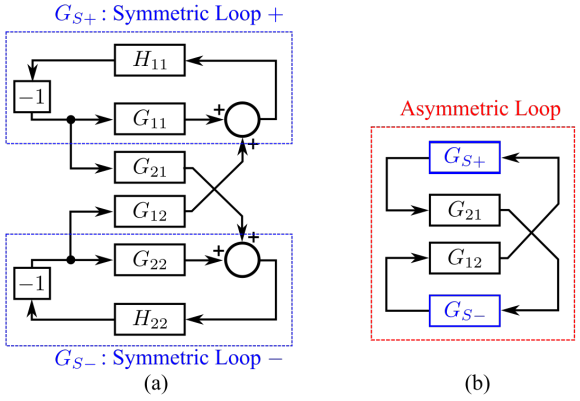

Fig. 12. Scalar block diagram for the closed-loop system when $\mathcal{H}$ is symmetric (i.e., when $H_{12} = H_{21} = 0$). The symmetric loops (a) and asymmetric loop (b) are visualized in blue and red dashed boxes respectively. Remarks: $G_{S+} = \frac{H_{11}}{1+G_{11}H_{11}}$; $G_{S-} = \frac{H_{22}}{1+G_{22}H_{22}}$; + and − branches are complex conjugate.

V. Example: A Droop-Controlled VSI

In this section, we give an example of how to apply the proposed theory in the modeling and analysis of a grid-connected droop-controlled VSI, and verify the major results by experiments.

The system under investigation is shown in Fig. 13(a) and (b). The dynamics of the VSI contains three parts [18]: filters (including inverter filters and grid impedance), inner control loops (voltage, current, and virtual impedance), and outer control loops (droop control). It has been demonstrated in [27] that the filters and inner loops can be collectively represented as an equivalent inductance-resistance in the mid-frequency range below the voltage loop bandwidth (usually a few hundred Hz). This leads to the simplified representation in Fig. 13(b) with a droop-controlled voltage source in series with L and R.

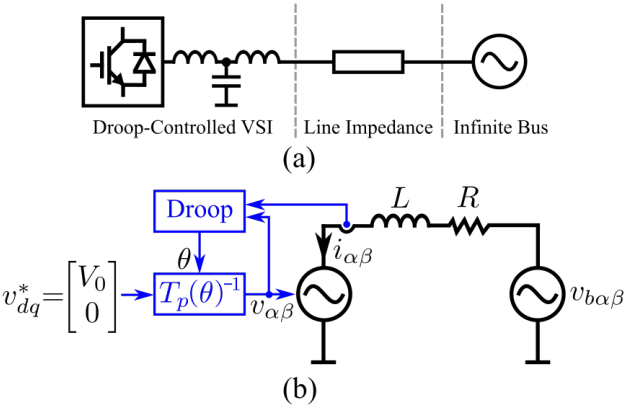

Fig. 13. Configuration of the system under investigation. (a) System layout. (b) Equivalent representation in the mid-frequency range.

A. Model Formulation

Now we model the dynamics of the system directly in the stationary frame. The state equation of the system in the $\alpha\beta\pm$ frame is

$$\begin{aligned}
\dot{i}_{\alpha\beta+}L &= -Ri_{\alpha\beta+} - v_{\alpha\beta+} + v_{b\alpha\beta+}\\
\dot{i}_{\alpha\beta-}L &= -Ri_{\alpha\beta-} - v_{\alpha\beta-} + v_{b\alpha\beta-}\\
\dot{\omega}_r\tau &= (\omega_0 - \omega_r) - m\cdot p\\
\dot{\theta} &= \omega_r.
\end{aligned} \quad (38)$$

The first two equations are governed by the Kirchhoff's law and the the second two equations are governed by the frequency droop control. The droop control measures output power $p = -(v_{\alpha\beta+}i_{\alpha\beta-} + v_{\alpha\beta-}i_{\alpha\beta+})/2$ and calculate the internal frequency ω_r and angle θ, which in turn governs the VSI voltage by $v_{\alpha\beta\pm} = V_0 e^{\pm j\theta}$. m is the droop gain and τ is the time constant of the low-pass filter in the droop control. V_0 and ω_0 denote the rated values of voltage and frequency, respectively.

Linearizing the state equation and applying Laplace transform, we get

$$\begin{aligned}
\hat{v}_{b\alpha\beta+}(s) &= Z_L(s)\hat{i}_{\alpha\beta+}(s) + jV_0\hat{\theta}(s_{-1})\\
\hat{v}_{b\alpha\beta-}(s) &= Z_L(s)\hat{i}_{\alpha\beta-}(s) - jV_0\hat{\theta}(s_1)\\
\hat{\theta}(s) &= M(s)(\hat{i}_{\alpha\beta+}(s_1) + \hat{i}_{\alpha\beta-}(s_{-1}))/V_0
\end{aligned} \quad (39)$$

in which

$$M(s) = \frac{mV_0^2}{2}(\tau s^2 + s - mV_0 I_0 \sin(\phi))^{-1},\ Z_L(s) = sL + R \quad (40)$$

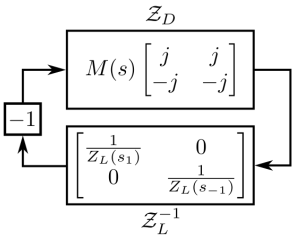

Fig. 14. Equivalent feedback system for the tested system.

and ϕ is the phase angle of the VSI current at the operating point. Substituting $\hat{\theta}(s)$ into the voltages in (39) yields

$$\begin{aligned}\hat{v}_{b\alpha\beta+}(s) &= [Z_L(s) + jM(s_{-1})]\,\hat{i}_{\alpha\beta+}(s) + jM(s_{-1})\,\hat{i}_{\alpha\beta-}(s_{-2}) \\ \hat{v}_{b\alpha\beta-}(s) &= [Z_L(s) - jM(s_1)]\,\hat{i}_{\alpha\beta-}(s) - jM(s_1)\,\hat{i}_{\alpha\beta+}(s_2).\end{aligned} \tag{41}$$

which is equivalent to

$$\begin{pmatrix} \hat{v}_{b\alpha\beta+}(s_1) \\ \hat{v}_{b\alpha\beta-}(s_{-1}) \end{pmatrix} = \underbrace{\begin{pmatrix} Z_L(s_1) + jM(s) & jM(s) \\ -jM(s) & Z_L(s_{-1}) - jM(s) \end{pmatrix}}_{\mathcal{Z}} \begin{pmatrix} \hat{i}_{\alpha\beta+}(s_1) \\ \hat{i}_{\alpha\beta-}(s_{-1}) \end{pmatrix}. \tag{42}$$

Equation (42) models the relationship between $\hat{i}_{\alpha\beta\pm}$ and $\hat{v}_{b\alpha\beta\pm}$, i.e., the port characteristics of the droop-controlled VSI in the stationary reference frame. The frequency coupling can be clearly seen from the frequency shifting in $\hat{v}_{\alpha\beta+}(s_1)$, $\hat{v}_{\alpha\beta-}(s_{-1})$, $\hat{i}_{\alpha\beta+}(s_1)$, and $\hat{i}_{\alpha\beta-}(s_{-1})$.

$\mathcal{Z}$ in (42) defines the total impedance of the grid-connected VSI system. It is of the same form as Fig. 5 from which follows the HTF and block-diagonalization immediately. $\mathcal{Z}$ can be re-written as

$$\mathcal{Z} = \underbrace{\begin{pmatrix} Z_L(s_1) & 0 \\ 0 & Z_L(s_{-1}) \end{pmatrix}}_{\mathcal{Z}_L} + \underbrace{M(s)\begin{pmatrix} j & j \\ -j & -j \end{pmatrix}}_{\mathcal{Z}_D} \tag{43}$$

which contains two parts. The first part $\mathcal{Z}_L$ is entry-diagonalized and takes the form of an inductance-resistance $Z_L(s) = sL + R$, which represents the dynamics of the inner loops, filters, and grid impedance. The second part $\mathcal{Z}_D$ is block-diagonalized and is proportional to $M(s)$, which represents the dynamics of droop control according to (40).

B. Stability Analysis

The diagonalized impedance model in the preceding subsection enables very convenient stability analysis, as shown below. Seen from the infinite bus of the grid, the stability of the grid-connected VSI is determined by the total admittance (the inversion of impedance):

$$\mathcal{Z}^{-1} = (\mathcal{Z}_L + \mathcal{Z}_D)^{-1} = (1 + \mathcal{Z}_L^{-1}\mathcal{Z}_D)^{-1}\mathcal{Z}_L^{-1}. \tag{44}$$

Since $\mathcal{Z}_L^{-1}$ is stable, we only need to consider $(1+\mathcal{Z}_L^{-1}\mathcal{Z}_D)^{-1}$, which could be formulated as an equivalent closed-loop system as shown in Fig. 14. This feedback system is of the same form as Fig. 9, if setting $\mathcal{G} = \mathcal{Z}_D$ and $\mathcal{H} = \mathcal{Z}_L^{-1}$. $\mathcal{Z}_D$ is asymmetric and $\mathcal{Z}_L^{-1}$ is symmetric, so we can use the simplified Mason's gain formula (37) to evaluate stability.

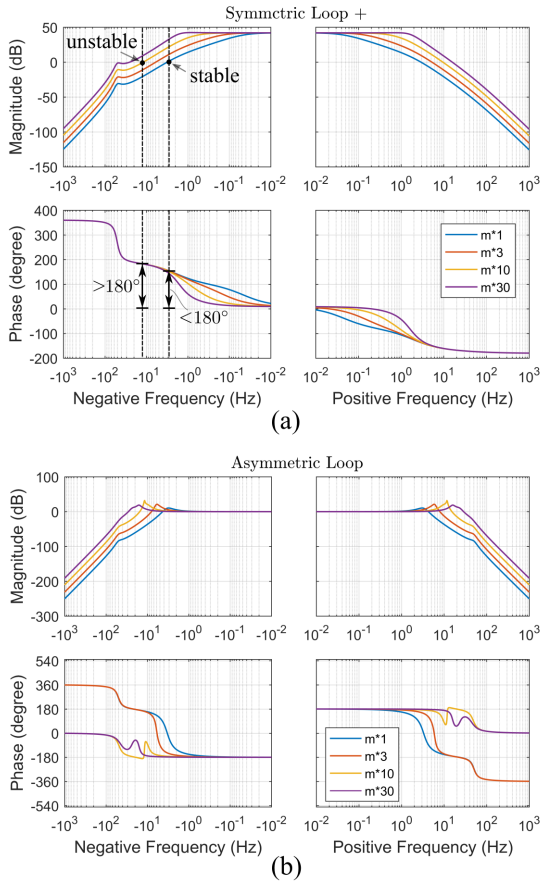

Fig. 15. Bode plots of loop gains for the symmetric and asymmetric loops for different values of droop gains. (a) Symmetric loop gain: $jM(s)/Z_L(s_1)$; only $+$ branch is shown here since the $+$ and $-$ branches are complex conjugate. (b) Asymmetric loop gain: $-G_{S+}G_{S-}M^2(s)$, where $G_{S+} = \frac{1/Z(s_1)}{1+jM(s)/Z_L(s_1)}$ and $G_{S-} = \frac{1/Z_L(s_{-1})}{1-jM(s)/Z_L(s_{-1})}$.

The Bode plots of the symmetric and asymmetric loops are embodied using the parameters in Table I and drawn in Fig. 15. It is clear from Fig. 15 (b) that the loop gain of the asymmetric loop is smaller than unity in almost all frequencies. Only for a very small range of frequencies, the loop gain is larger than unity but the corresponding phase margins are positive. Therefore, the asymmetric loop is stable and the quasi-symmetric condition described in Section IV is met. This property allows us to focus on the symmetric loop, which enables significant simplification of stability analysis and control design.

The symmetric loop has higher gain and may indeed cause instability, as shown in Fig. 15 (a). As the droop gain m increases, the phase margin decreases, from which we get the critical gain which agrees with the result in [18], [19]. Further observation on the symmetric loop shows that $Z(s_{\pm 1})$ (entries of $\mathcal{Z}_L$) are passive yet $\pm jM(s)$ (entries of $\mathcal{Z}_D$) are non passive. It is this non-passivity that induces the $> 180^\circ$ phase shift in the loop gain and has a destabilizing

TABLE I
PARAMETERS OF THE EXPERIMENT SYSTEM.

Rated frequency	$\omega_0 = 1$ pu
VSI voltage	$V_0 = 1$ pu
VSI current	$I_0 = 0.30$ pu
Current Angle	$\phi = 188°$
Net inductance	$L = 0.091$ pu
Net resistance	$R = 0.015$ pu
Rated droop gain	$m_{rated} = 2\%\omega_{base}/S_{base}$
Low-pass filter time constant	$\tau = 1/(2\pi \cdot 2)$ s/rad
Voltage-loop bandwidth	300 Hz
Base values for per-unit (pu) system: $S_{base} = 10$kVA, $V_{base} = 380$V, $I_{base} = S_{base}/V_{base}$, $\omega_{base} = 2\pi \times 50$ rad/s, $Z_{base} = V_{base}/I_{base}$, $L_{base} = Z_{base}/\omega_{base}$	

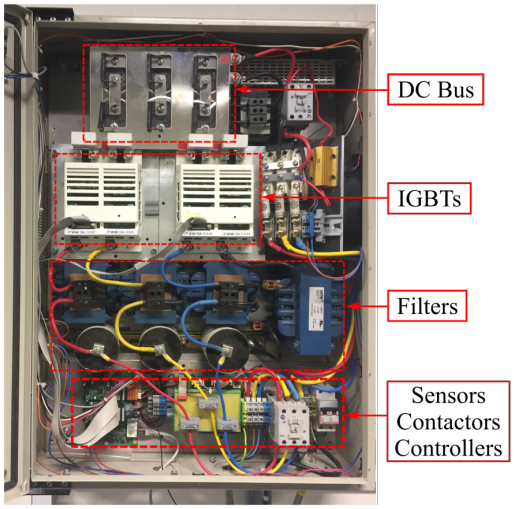

Fig. 16. Photo of the droop-controlled VSI.

(negative damping) effect on the system when the droop gain is excessively high [28], [29]. Thus we get a better understanding than [18], [19] on the mechanism of instability of drooped-controlled VSI systems.

C. Experiment Verification

A experimental platform was built to test the system in Fig. 13(a), with the parameters listed in Table I. The detailed control structure is same as the one used for a conventional droop-controlled VSI [18], which is equivalently to Fig. 13(b) in the investigated frequency range. The photo of the VSI is shown in Fig. 16. The droop gain m is set to be below and about the critical value and the corresponding dynamic responses are recorded in Fig. 17. When the droop gain m is set to the rated value ($m_{rated} = 2\%\omega_{base}/S_{base}$), the system is stable. By contrast, when m is set to 10 times the rated value ($10m_{rated}$), the phase margin becomes negative (see Fig. 15) and the system becomes unstable. This result confirms the accuracy of the stability criterion derived from the diagonalized HTF in the preceding subsection.

A Simulink model was also built to measure the total admittance ($\mathcal{Z}_T^{-1}$) of the tested system via frequency sweeping,

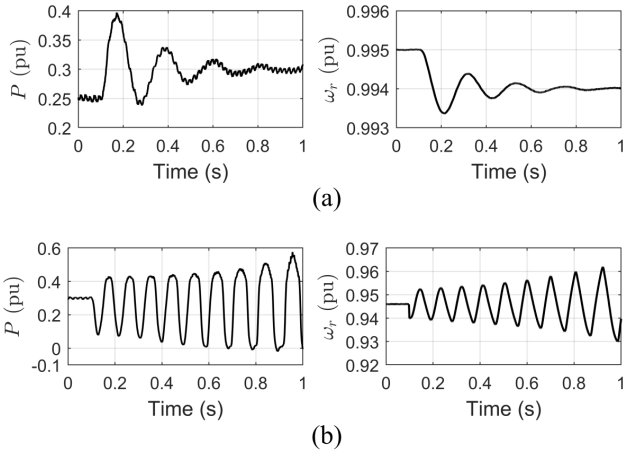

Fig. 17. Experimental testing of VSI step response. (a) For droop gain of $m = m_{rated}$. (b) With droop gain increased to $m = 10m_{rated}$

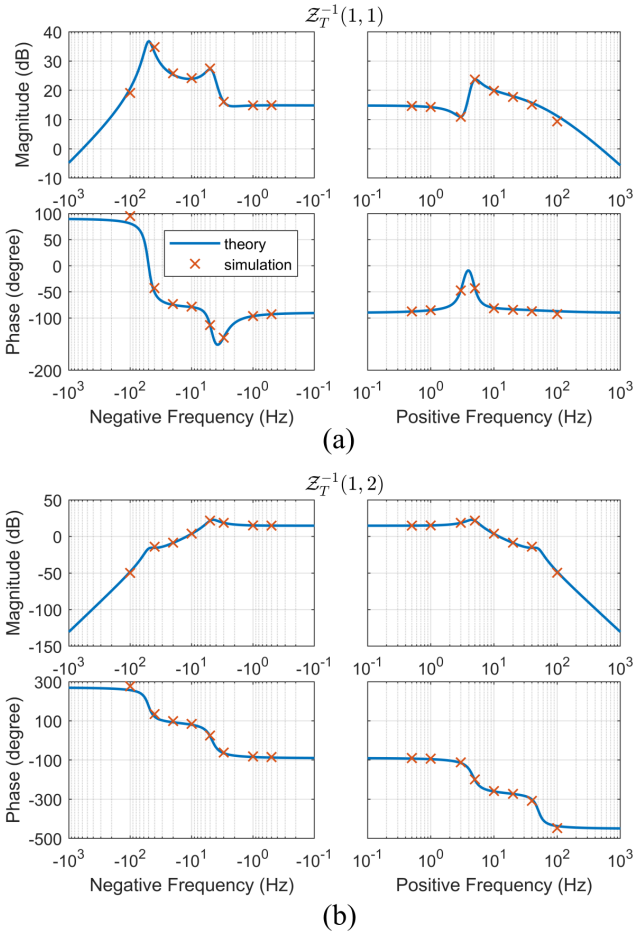

Fig. 18. Admittance spectrum of the droop-controlled VSI measured by frequency sweeping. (a) Diagonal entry $[\mathcal{Z}_T^{-1}(1,1)]$. (b) Off-diagonal entry $[\mathcal{Z}_T^{-1}(1,2)]$.

and the measured values are compared with theoretic models, as shown in Fig. 18. The models are derived in the stationary frame using HTF diagonalization, and the measurement is conducted in the synchronous frame. Again, very close matching is observed in both the gain and phase including all the key features of poles and zeros. There is a minor discrepancy at $\pm 10^2$Hz and this is due to the sampling delay and spectrum leakage in the admittance measurement algorithm. The frequency sweeping results further verify the accuracy of the proposed theory.

VI. Conclusions

A correspondence between frame transformations and harmonic transfer functions (HTFs) has been established. Frame transformations are proved to be equivalent to similarity transformations on HTF matrices, which have a diagonalization effect under certain conditions. The diagonalization takes place in two steps: block-diagonalization via rotation transformation for balanced sinusoidal systems, and entry-diagonalization via complex transformation for symmetric systems. The diagonalization essentially reduced the order of an HTF matrix from infinity to two or one and thereby makes the matrix tractable mathematically without truncation or approximation. A case study of a droop-controlled grid-connected voltage source inverter (VSI) demonstrates the practical benefits of the proposed theory. The droop-controlled VSI proves to be quasi-symmetric (entry-diagonalizable) which leads to significant simplification of stability analysis and sheds new light on the mechanism of instability. Moreover, the proposed linkage opens up new possibilities of looking for other frame transformations beyond the basic transformations (rotating, complex) to extend the diagonalization method to asymmetric, unbalanced, and non-sinusoidal systems.

References

[1] W. C. Duesterhoeft, M. W. Schulz, and E. Clarke, "Determination of Instantaneous Currents and Voltages by Means of Alpha, Beta, and Zero Components," *Transactions of the American Institute of Electrical Engineers*, vol. 70, no. 2, pp. 1248–1255, July 1951.

[2] K. W. Martin, "Complex signal processing is not complex," *IEEE Transactions on Circuits and Systems I: Regular Papers*, vol. 51, no. 9, pp. 1823–1836, 2004.

[3] J. Holtz, "The representation of AC machine dynamics by complex signal flow graphs," *IEEE Transactions on Industrial Electronics*, vol. 42, no. 3, pp. 263–271, June 1995.

[4] L. Harnefors, "Modeling of three-phase dynamic systems using complex transfer functions and transfer matrices," *IEEE Transactions on Industrial Electronics*, vol. 54, no. 4, pp. 2239–2248, 2007.

[5] R. H. Park, "Two-reaction theory of synchronous machines generalized method of analysis-part I," *Transactions of the American Institute of Electrical Engineers*, vol. 48, no. 3, pp. 716–727, July 1929.

[6] Y. Li, *AC motor digital control system*. Machinery Industry Press, 2012.

[7] D. Hume, A. Wood, and C. Osauskas, "Frequency-domain modelling of interharmonics in HVDC systems," *IEE Proceedings-Generation, Transmission and Distribution*, vol. 150, no. 1, pp. 41–48, 2003.

[8] J. Lyu, X. Zhang, X. Cai, and M. Molinas, "Harmonic state-space based small-signal impedance modeling of a modular multilevel converter with consideration of internal harmonic dynamics," *IEEE Transactions on Power Electronics*, vol. 34, no. 3, pp. 2134–2148, March 2019.

[9] X. Wang and F. Blaabjerg, "Harmonic stability in power electronic based power systems: concept, modeling, and analysis," *IEEE Trans. Smart Grid*, pp. 1–1, 2018.

[10] X. Wang, F. Blaabjerg, and W. Wu, "Modeling and analysis of harmonic stability in an AC power-electronics-based power system," *IEEE Transactions on Power Electronics*, vol. 29, no. 12, pp. 6421–6432, 2014.

[11] N. M. Wereley and S. R. Hall, "Frequency response of linear time periodic systems," in *Decision and Control, 1990., Proceedings of the 29th IEEE Conference on*. IEEE, 1990, pp. 3650–3655.

[12] N. M. Wereley, "Analysis and control of linear periodically time varying systems," Ph.D. dissertation, Massachusetts Institute of Technology, 1990.

[13] S. R. Hall and N. M. Wereley, "Generalized Nyquist stability criterion for linear time periodic systems," in *1990 American Control Conference*. IEEE, 1990, pp. 1518–1525.

[14] G. N. Love and A. R. Wood, "Harmonic state space model of power electronics," in *2008 13th International Conference on Harmonics and Quality of Power*. IEEE, 2008, pp. 1–6.

[15] J. Mahdavi, A. Emaadi, M. Bellar, and M. Ehsani, "Analysis of power electronic converters using the generalized state-space averaging approach," *IEEE Transactions on Circuits and Systems I: Fundamental Theory and Applications*, vol. 44, no. 8, pp. 767–770, 1997.

[16] J. Sun, "Small-signal methods for AC distributed power systems–a review," *IEEE Transactions on Power Electronics*, vol. 24, no. 11, pp. 2545–2554, 2009.

[17] X. Yue, X. Wang, and F. Blaabjerg, "Review of small-signal modeling methods including frequency-coupling dynamics of power converters," *IEEE Transactions on Power Electronics*, pp. 1–1, 2018.

[18] N. Pogaku, M. Prodanovic, and T. C. Green, "Modeling, analysis and testing of autonomous operation of an inverter-based microgrid," *IEEE Trans. Power Electron.*, vol. 22, no. 2, pp. 613–625, Mar. 2007.

[19] E. Barklund, N. Pogaku, M. Prodanovic, C. Hernandez-Aramburo, and T. C. Green, "Energy management in autonomous microgrid using stability-constrained droop control of inverters," *IEEE Transactions on Power Electronics*, vol. 23, no. 5, pp. 2346–2352, Sep. 2008.

[20] P. Khargonekar, K. Poolla, and A. Tannenbaum, "Robust control of linear time-invariant plants using periodic compensation," *IEEE Transactions on Automatic Control*, vol. 30, no. 11, pp. 1088–1096, 1985.

[21] M. M. Seron, J. H. Braslavsky, and G. C. Goodwin, *Fundamental limitations in filtering and control*. Springer Science & Business Media, 2012.

[22] B. Wen, D. Dong, D. Boroyevich, R. Burgos, P. Mattavelli, and Z. Shen, "Impedance-based analysis of grid-synchronization stability for three-phase paralleled converters," *IEEE Transactions on Power Electronics*, vol. 31, no. 1, pp. 26–38, Jan 2016.

[23] L. Harnefors, M. Bongiorno, and S. Lundberg, "Input-admittance calculation and shaping for controlled voltage-source converters," *IEEE transactions on industrial electronics*, vol. 54, no. 6, pp. 3323–3334, 2007.

[24] X. Wang, L. Harnefors, and F. Blaabjerg, "Unified impedance model of grid-connected voltage-source converters," *IEEE Transactions on Power Electronics*, vol. 33, no. 2, pp. 1775–1787, 2018.

[25] S. J. Mason, "Feedback theory: Further properties of signal flow graphs," 1956.

[26] J. Pliam and E. B. Lee, "On the global properties of interconnected systems," *IEEE Transactions on Circuits and Systems I: Fundamental Theory and Applications*, vol. 42, no. 12, pp. 1013–1017, 1995.

[27] Y. Gu, N. Bottrell, and T. C. Green, "Reduced-order models for representing converters in power system studies," *IEEE Transactions on Power Electronics*, vol. 33, no. 4, pp. 3644–3654, 2018.

[28] Y. Gu, W. Li, and X. He, "Passivity-based control of DC microgrid for self-disciplined stabilization," *IEEE Transactions on Power Systems*, vol. 30, no. 5, pp. 2623–2632, 2015.

[29] L. Harnefors, X. Wang, A. G. Yepes, and F. Blaabjerg, "Passivity-based stability assessment of grid-connected VSCs – an overview," *IEEE Journal of Emerging and Selected Topics in Power Electronics*, vol. 4, no. 1, pp. 116–125, March 2016.

Yitong Li (S'17) received the B.Eng degrees from Huazhong University of Science and Technology, China, and the University of Birmingham, UK, in 2015. He received his M.Sc degree in Future Power Networks from Imperial College London, UK, in 2016, where he is currently pursuing his Ph.D. degree. His current research interests include control techniques and power electronic converters for power distribution applications.

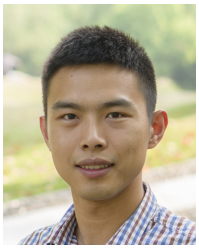

Yunjie Gu (M'18) received the B.Sc. and the Ph.D. degree in Electrical Engineering from Zhejiang University, Hangzhou, China, in 2010 and 2015 respectively. He was a Research Consultant at General Electric Global Research Centre, Shanghai, from 2015 to 2016, and is now an EPSRC-funded Innovation Fellow at Imperial College London (award EP/S000909/1). His research interests include power system control and stability, and the application of power electronics to power systems.

Timothy C. Green (M'89-SM'02-F'19) received a B.Sc. (Eng) (first class honours) from Imperial College London, UK in 1986 and a Ph.D. from Heriot-Watt University, Edinburgh, UK in 1990. He is a Professor of Electrical Power Engineering at Imperial College London, and Director of the Energy Futures Lab with a role fostering interdisciplinary energy research. His research interest is in using the flexibility of power electronics to accommodate new generation patterns and new forms of load, such as EV charging, as part of the emerging smart grid. In HVDC he has contributed converter designs that reduce losses while also providing control functions assist AC system integration. In distribution systems, he has pioneered the use of soft open points and the study of stability of grid connected inverters. Prof. Green is a Chartered Engineering the UK and a Fellow of the Royal Academy of Engineering.